Optical Injection Locking of Longitudinal Modes in a Discrete Mode Laser: Application in Gain-Switched Optical Frequency Combs

Ana Quirce, Bryan Kelleher, and Angel Valle

***Abstract*—A detailed experimental study of the effect of external optical injection (OI) on a single-mode discrete mode laser (DML) when the wavelength of the OI is far from that of the solitary DML is presented. We show that the situation observed in Fabry Pérot lasers by Jain et al. extends to single-mode DMLs since injection locking of many longitudinal modes of the device is obtained, giving rise to a wavelength tunability larger than 37 nm. We show that the injection locking range is minimum when injecting close to the longitudinal mode that appears in the free-running DML ($q = 0$). We present the observed nonlinear dynamics of the laser when subject to OI with a wavelength close to a longitudinal mode with $q \neq 0$ and in particular, we show that OI induces dynamics simultaneously in several longitudinal modes. Different nonlinear dynamics are observed for positive and negative frequency detunings with respect to the injected mode. We also investigate the effect of OI in optical frequency combs (OFCs) generated by gain-switching the DML in a very wide range of wavelengths of the OI. We show that wavelength tunable injection-locked OFCs are obtained with quasi-continuous wavelength tunability larger than 37 nm.**

***Index Terms*—Gain switching, injection locking, longitudinal modes, optical frequency comb generator, optical injection, semiconductor lasers.**

I. Introduction

SINGLE-MODE semiconductor lasers have found wide application in optical communications, sensing, metrology, and spectroscopy. The discrete mode laser (DML), in which a small number of refractive index perturbations are introduced in a Fabry-Pérot laser cavity, offers a simple regrowth free path to single-mode laser operation [1], [2], [3], [4], [5], [6], [7], [8], [9]. DMLs advantages include narrow linewidth [4], and robustness against feedback [10]. The usual DMLs are 1.3 and 1.55 μm wavelength InGaAsP devices. Index-patterned nitride lasers can stand out in terms of single mode operation [11]. Also silicon-photonics integrated lasers have been obtained using the index-patterned concept [12].

Optical injection of laser light (OI) in semiconductor lasers has been studied for many years [13], [14], [15]. Optical injection locking can improve the laser emission characteristics by enhancing the intrinsic modulation frequency response and by reducing the noise and the frequency chirp [14]. OI in continuous wave (CW) single-mode lasers is also of interest because it induces a wide variety of nonlinear dynamical regimes, including four-wave mixing, periodic and chaotic behaviours and injection locking [14].

Semiconductor lasers can also be used to generate Optical Frequency Combs (OFCs). These are coherent light sources consisting of a series of evenly spaced and coherent discrete spectral components. OFCs find applications in frequency metrology, high accuracy spectroscopy [16], high-speed optical communications [17], [18], [19], optical ranging [20], gas-sensing [21], [22], and optical arbitrary waveform generation [23]. Advantages of generating OFCs with laser diodes include small footprint, high efficiency, and low cost. Several approaches have been used to generate OFCs in semiconductor lasers: electro-optic modulation [24], micro-ring resonators [25], mode-locking [26], and gain switching (GS) [27]. The GS technique consists of the application of a periodic radio-frequency (RF) large signal modulation superimposed to a direct bias current. Considerable attention has been paid to GS-OFCs [18], [19], [27], [28], [29], [30], [31], [32], [33], [34], [35], [36], [37], [38], [39], [40] since they have additional advantages like easy implementation, low losses, flexibility in the selection of the frequency spacing, compactness, and low energy consumption [27]. Applications of OFCs generated by GS include multi-carrier optical communications [17], [18], [41], [42], [43], sub-THz generation [44], radio-over-fiber [19], low noise microwave generation [45] and absorption spectroscopy [35], [36], [46].

The effect of OI from a CW laser (ML) into GS-OFCs of single-mode lasers has also been analyzed. In this case OI can improve the spectral characteristics of the OFCs when performed under specific injection conditions. For instance, OI can transform a broad noisy optical spectrum from a GS single-mode laser into a high quality OFC [27], [37]. Also

Manuscript received 29 November 2023; revised 31 January 2024; accepted 5 February 2024. Date of publication 8 February 2024; date of current version 16 May 2024. The work of Ana Quirce supported by Beatriz Galindo Program, Ministerio de Ciencia, Innovación y Universidades (Spain). This work was supported by the Ministerio de Ciencia e Innovación, Spain, under Grant PID2021-123459OB-C22 MCIN/AEI/10.13039/501100011033/FEDER,UE. *(Corresponding author: Angel Valle.)*

Ana Quirce and Angel Valle are with the Instituto de Física de Cantabria (IFCA) (Universidad de Cantabria-CSIC), E39005 Santander, Spain (e-mail: quirce@ifca.unican.es; valle@ifca.unican.es).

Bryan Kelleher is with the School of Physics, University College Cork, T12 K8AF Cork, Ireland, and also with the Tyndall National Institute, University College Cork, T12 R5CP Cork, Ireland (e-mail: bryan.kelleher@ucc.ie).

Color versions of one or more figures in this article are available at https://doi.org/10.1109/JLT.2024.3363892.

Digital Object Identifier 10.1109/JLT.2024.3363892

© 2024 The Authors. This work is licensed under a Creative Commons Attribution 4.0 License. For more information, see https://creativecommons.org/licenses/by/4.0/

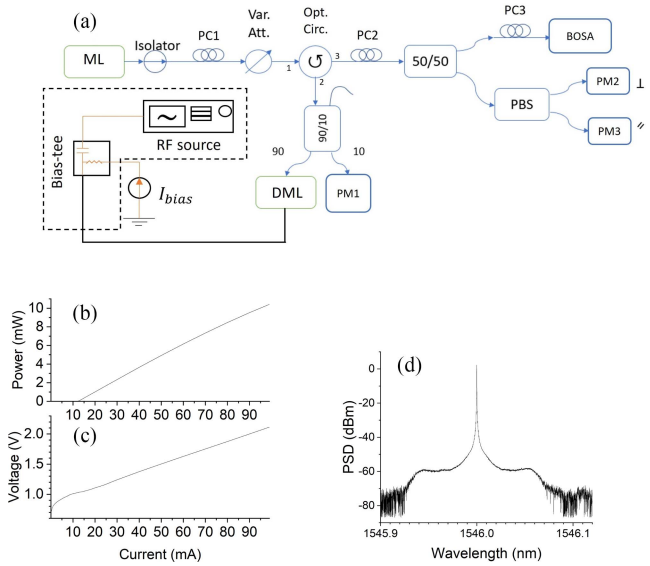

Fig. 1. (a) Experimental setup for performing optical injection in GS operation. ML: master laser, DML: discrete mode laser, PC: polarization controller, PM: power meter, PBS: polarization beam splitter, BOSA: Brillouin optical spectrum analyzer, (b) Power-current Characteristics, (c) Voltage-current Characteristics, and (d) Optical spectrum at I_{bias}= 30 mA.

significant reduction of the linewidth of individual comb lines is obtained when using a narrow linewidth primary laser, because this low linewidth is transferred to the OFC lines [32], [37], [47]. It has also been shown that the locking range for GS lasers is considerably greater than that corresponding to CW lasers because the OFC can be locked by injecting close to several of the central lines of the comb [32], [48]. Detrimental characteristics like timing jitter, small values of carrier-to-noise ratio (CNR), small pulse-to-pulse phase correlation, and RIN, can also be improved by using appropriate OI [27], [29], [31], [32], [39], [49], [50].

Most of the above mentioned works concern of the effect of external OI with a wavelength close to that of the longitudinal mode of the solitary single-mode laser. This situation also holds in the experimental and theoretical analysis of the nonlinear dynamics of single-mode laser diodes subject to OI [14]. Also the effect of OI in GS-OFCs has usually been analyzed when the wavelength of the injecting laser is close to one of the lines of the comb generated around that longitudinal mode [27], [38], [39], [48]. Most of these investigations have been performed using single-mode lasers like Distributed Feedback Lasers (DFBs) or DMLs. However, multi-mode lasers have also been recently considered in an experimental investigation of the effect of OI in gain-switched Fabry-Pérot (FP) semiconductor laser [40]. In this work wavelength tunable optical frequency comb generation was demonstrated with a very wide wavelength tunable-range: a quasi-continuous wavelength tunability of 31 nm was demonstrated [40]. This wide tunability is due to the excitation of the different longitudinal modes of the FP laser due to the external OI.

In this article we experimentally study the effect of external OI in a single-mode DML when the injecting wavelength is far from that of the solitary DML. We show that the situation observed in FP lasers [40], extends to single-mode DMLs since injection locking of many longitudinal modes of the device can be obtained, giving rise to a wavelength tunability range larger than 37 nm. The advantage of using DMLs is that off-the-shelf devices are high-frequency connectorized. In contrast, off-the-shelf FP lasers are not usually high-frequency connectorized although some commercial devices reach high frequency response up to 25 GHz [40]. We describe the nonlinear dynamics of the DML laser when subject to OI with a wavelength close to a longitudinal mode different from that observed in the solitary laser. We also analyze the effect of OI in OFCs generated by gain-switching DMLs over a very wide range of injected wavelengths. We show that wavelength tunable OFCs generation are obtained with a quasi-continuous wavelength tunability larger than 37 nm.

The paper is organized as follows. In Section II we describe the experimental set-up. Section III is devoted to the description of the effect of OI on the CW-DML. In Section IV we analyze the nonlinear dynamics of the DML far from the longitudinal mode of the solitary DML. Section V is devoted to the effect of OI on GS-OFCs generated in the DML. Finally, in Section VI we discuss and summarize our results.

II. Experimental Techniques

In this section a 10 GHz-bandwidth DML (Eblana Photonics EP1550-0-DM-H19-FM) emitting at a wavelength close to 1550 nm is subject to CW-OI by using the setup shown in Fig. 1(a). The DML is a multi-quantum well device in a ridge waveguide with index perturbations, in order to allow single-mode operation [51]. The device is packaged in a 7-pin butterfly with high frequency input connectors and does not have a built-in optical isolator in order to allow external optical injection. The CW bias current, I_{bias}, and the temperature of the DML were controlled with a laser driver and a temperature controller (Luzwavelabs LDC/E-Current200 and LDC/E-Temp3), respectively. The temperature of the DML was held constant at 15 °C. At this temperature the threshold current of the DML is I_{th} = 12.3 mA. Power-current and voltage-current characteristics are shown in Fig. 1(b) and (c), respectively. The bias injection current was set at I_{bias} = 30 mA, for which the relaxation oscillation frequency is 6.3 GHz. The optical spectrum at that current is shown in Fig. 1(d). The GS operation of the DML considered in Section V is obtained by the superposition, via a bias-tee, of I_{bias} and a sinusoidal modulation current at f_R = 5 GHz frequency provided by an RF generator (Keysight N5173B).

Light from a tunable laser (Pure Photonics PPCL300), with a narrow linewidth (75 kHz), was injected into the DML via an optical circulator. At the output of the master laser an optical isolator is included to avoid optical feedback in the device. A polarization controller (PC1) was used for maximizing the power injected into the DML. The amount of light injected into the DML was controlled by a variable optical attenuator. The second port of the circulator is connected to a 90/10 fiber coupler. The 90% branch is connected to the DML. The 10% branch is

connected to a power meter to monitor the injected power. The optical injection is characterized by its strength, given by the value of the power measured in front of the DML, P_i, and by its optical wavelength (frequency), λ_i (ν_i). The output of the DML is analyzed by connecting the third port of the circulator to a second PC (PC2) and a 50/50 coupler. A polarization beam splitter (PBS) and two power meters are included to perform the maximization process of the power injected into the DML, ensuring in this way that the polarizations of both the DML and the injected light coincide. The optical spectrum of the DML is measured with a high-resolution (10 MHz) Brillouin optical spectrum analyser (BOSA) (Aragon Photonics BOSA 210). The emission wavelength (frequency) of the DML with no optical injection is λ_0 =1546.001 nm ($\nu_0 = 194.049$ THz) at $I_{bias} = 30$ mA. The frequency separation between consecutive longitudinal modes is $\delta\nu = 156.14$ GHz that corresponds to a wavelength separation of $\delta\lambda = c\delta\nu/\nu_0^2 = 1.244$ nm. The optical frequency of the $q-$longitudinal mode of the DML is $\nu_q = \nu_0 - q\delta\nu$, where q is an integer. The corresponding wavelength is $\lambda_q = c/\nu_q$, that can be approximated by $\bar{\lambda}_q = \lambda_0 + q\delta\lambda$, providing that $q\delta\nu/\nu_0 << 1$. Since for large values of q the error of the previous approximation can be appreciable (for instance, $\lambda_{15} - \bar{\lambda}_{15} = 0.228$ nm) we will define the wavelength detuning using λ_q. In this way the wavelength (frequency) detuning between the optical injection and the $q-$longitudinal mode of the DML is given by $\Delta\lambda_q = \lambda_i - \lambda_q$ ($\Delta\nu_q = \nu_i - \nu_q$).

III. Effect of the Optical Injection on the CW-DML

In our first experiment we fix the OI wavelength to λ_i = 1541.050 nm and change the attenuation level in order to increase P_i. The wavelength (frequency) detuning with respect to the $q = -4$ longitudinal mode is $\Delta\lambda_{-4} = 0.009$ nm ($\Delta\nu_{-4} = -1.1$ GHz). Fig. 2 shows the optical spectra obtained for six different values of P_i. When P_i is very small the spectrum is mainly composed of two lines appearing at λ_i and λ_0, as can be seen in Fig. 2(a). Fig. 2(b) shows that the strength of the peak at λ_i increases as P_i is increased. Also, increasing P_i induces a larger amount of stimulated recombination of carriers, and hence a smaller carrier density. In this way the refractive index and the wavelength of the $q = 0$ mode in the presence of injection, λ_0', increase with P_i ($\lambda_0' = 1546.016$ nm in Fig. 2(b)). A small peak also appears at a wavelength close to 1551 nm. The origin of this peak is now discussed when considering a larger value of P_i, as shown in Fig. 2(c). In this Figure an extra peak also appears at a 1536.127 nm wavelength. The optical frequencies of the peaks, from left to right in Fig. 2(c), are 195.2964, ν_i =194.6725, ν_0' =194.0470 and 193.4225 THz. The frequency difference between consecutive lines is nearly constant, around 0.6245 THz, so the previous frequencies appears at $2\nu_i - \nu_0'$, ν_i, ν_0', and $2\nu_0' - \nu_i$, respectively. In this way there is beating between lines that indicates that there is some coherence between the spectral lines. The frequency (wavelength) separation between consecutive lines is 0.6245 THz ($\sim$4.96 nm) that is very close to $4\delta\nu$ ($4\delta\lambda$). This suggests that the four lines correspond to the excitation of $q = -8$, -4, 0, and $q = 4$ longitudinal modes. This is confirmed when assuming that the wavelength shift of the

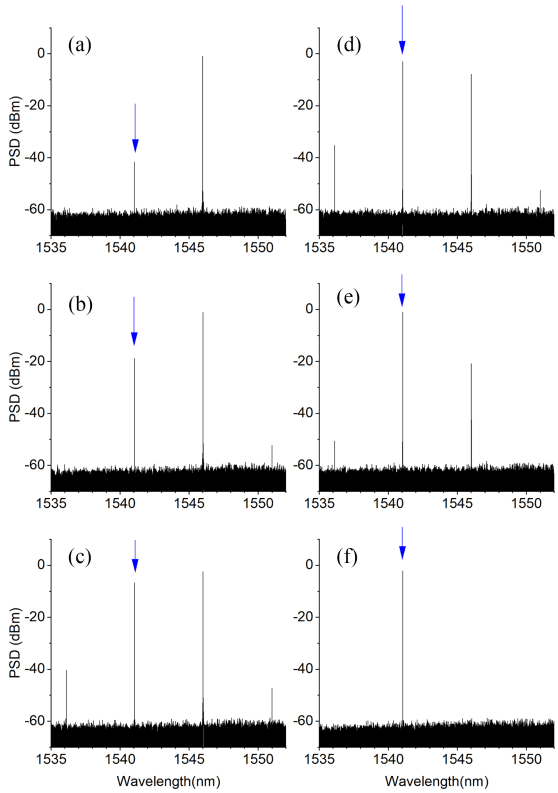

Fig. 2. Optical spectra at $\Delta\nu_{-4} = -1.1$ GHz for (a) $P_i = 7.3$ nW, (b) $P_i = 2.6\,\mu$W, (c) $P_i = 34.8\,\mu$W, (d) $P_i = 84.9\,\mu$W, (e) $P_i = 106.9\,\mu$W, and (f) $P_i = 268.6\,\mu$W. The injection wavelength is indicated with an arrow.

longitudinal modes when increasing P_i is similar to that measured for the $q = 0$ mode. When doing this, the detuning frequency in the presence of the optical injection, $\Delta\nu_{-4}' = \nu_i - \nu_{-4}'$, is 0.9, 1, 1.3, and 5.2 GHz for Fig. 2(b), (c), (d), and (e), respectively. This indicates that the appreciable excitation of the $q = -8$ and $q = 4$ longitudinal modes occurs when ν_i is close to ν_{-4}' (see Fig. 2(d)) and begins to disappear as ν_i moves away from ν_{-4}' (see Fig. 2(e)). Fig. 2(f) shows that for large values of P_i the DML is locked to the optical injection as only the peak at λ_i appears in the spectrum.

We now analyze if the locking situation illustrated in Fig. 2(f) extends to longitudinal modes with large values of $\mid q \mid$. In order to do this we increase the injected power P_i to 8.2 mW. Fig. 3 shows several optical spectra obtained for different q for which injection locking is observed. This locking is observed for all longitudinal modes with q between -15 and 15. We can not observe locking beyond those values since the wavelengths are beyond the wavelength range that can be measured with our optical spectrum analyzer. These results indicate that injection locking can be obtained in a wavelength range of 37.5 nm (and likely larger).

While phase locking is obtained around each longitudinal mode, there are also regions of unlocked and dynamical behaviour. For the conditions of Fig. 3, phase-locking is observed for a significant range - around 45% of the 37.5 nm. This percentage is expected to increase as P_i increases. The wavelength range around each mode over which locking is observed is not

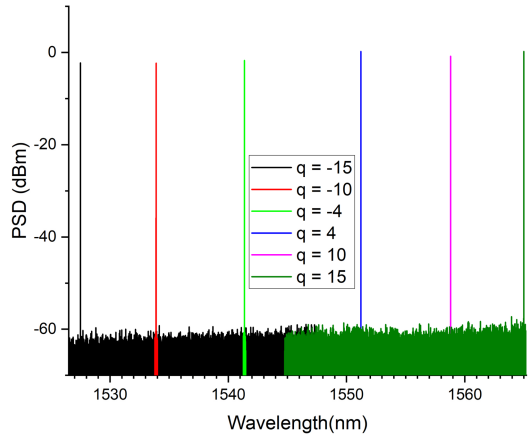

Fig. 3. Optical spectra of the DML at $P_i = 8.22$ mW for several values of the injected wavelength: $\Delta\lambda_{-15} = -0.074$ nm (black), $\Delta\lambda_{-10} = 0.229$ nm (red), $\Delta\lambda_{-4} = 0.329$ nm (green), $\Delta\lambda_4 = 0.227$ nm (blue), $\Delta\lambda_{10} = 0.258$ nm (magenta), and $\Delta\lambda_{15} = 0.111$ nm (olive).

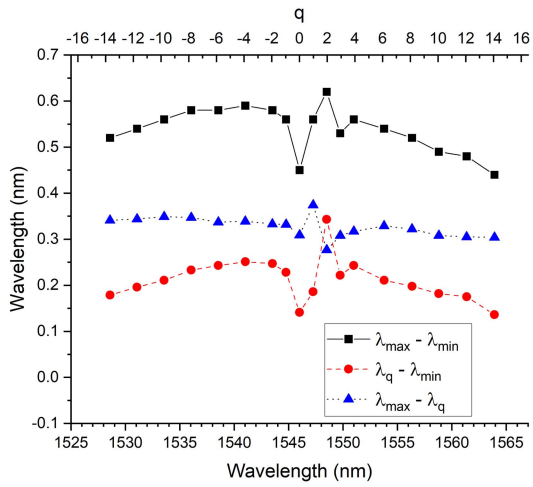

Fig. 4. Injection locking range for positive $\Delta\lambda_q$ (triangles), and negative $\Delta\lambda_q$ (circles) vs. longitudinal mode wavelength. The total locking range is also plotted with squares. In this figure $P_i = 8.2$ mW.

symmetric. Some examples with positive and negative values of $\Delta\lambda_q$ are illustrated in Fig. 3. Experimental and theoretical analysis have shown that the locking range is larger for positive $\Delta\lambda_0$ than for negative $\Delta\lambda_0$ [14]. We now extend these analysis for values of $q \neq 0$. We define $(\lambda_{\min}, \lambda_{\max})$ as the interval in which the locking is observed around λ_q. We show in Fig. 4 the values of $\lambda_q - \lambda_{\min}$ and $\lambda_{\max} - \lambda_q$ as a function of the wavelength (or as a function of q in the upper axis). These results show that the locking range for positive $\Delta\lambda_q$, $\lambda_{\max} - \lambda_q$, is larger than the range for negative $\Delta\lambda_q$, $\lambda_q - \lambda_{\min}$, with the only exception of $q = 2$. The range for positive $\Delta\lambda_q$ remains constant with q with the exception of $q = 0, 1$, and 2 in which there are small relative minimum, maximum and minimum, respectively. The range for negative $\Delta\lambda_q$ has a minimum, maximum and minimum, when $q = 0, 2$, and 3, respectively. This range increases (decreases) with the wavelength for $q < -2$ ($q > 4$). The total injection locking range, $\lambda_{\max} - \lambda_{\min}$, is obtained by adding the previous two ranges, $\lambda_{\max} - \lambda_q$ and $\lambda_q - \lambda_{\min}$, and is also plotted in Fig. 4. The total locking range has a clear minimum at $q = 0$ (0.45 nm, 56.2 GHz) since both, $\lambda_q - \lambda_{\min}$ and $\lambda_{\max} - \lambda_q$ have also a minimum at $q = 0$. The maximum locking range appears for $q = 2$ (0.62 nm, 77.6 GHz) due to the clear maximum of $\lambda_q - \lambda_{\min}$ at that q value. Results in Fig. 4 indicate that the most analyzed case in the literature, $q = 0$, is precisely the case in which the injection locking range is minimum.

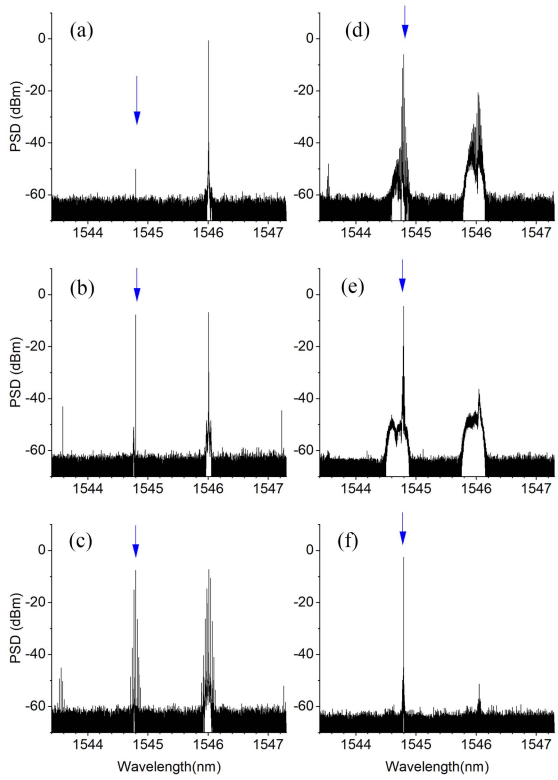

Fig. 5. Optical spectra at $\Delta\nu_{-1} = -5.2$ GHz for (a) $P_i = 7.3$ nW, (b) $P_i = 84.9\,\mu$W, (c) $P_i = 134.6\,\mu$W, (d) $P_i = 194.6\,\mu$W, (e) $P_i = 213.4\,\mu$W, and (f) $P_i = 218.4\,\mu$W. The injection wavelength is indicated with an arrow.

IV. Nonlinear Dynamics of the CW-DML Subject to OI Far From the Free-Running Longitudinal Mode

In this section we analyze the nonlinear dynamics of the DML when injecting close to a longitudinal mode different from the mode emitted by the solitary laser ($q = 0$). We first analyze the case in which the frequency detuning with respect to the longitudinal mode is negative. In this way we fix the OI wavelength to $\lambda_i = 1544.8$ nm, close to λ_{-1}, and change the attenuation level in order to increase P_i. The frequency detuning with respect to the $q = -1$ longitudinal mode is $\Delta\nu_{-1} = -5.2$ GHz ($\Delta\lambda_{-1} = 0.042$ nm). While in Fig. 2 the attenuation step was 1 dB, now the attenuation step is 0.1 dB in order to appreciate the transitions between different nonlinear dynamics of the system. Fig. 5 shows the optical spectrum obtained for six different values of P_i.

Fig. 5(a) shows that when P_i is small a peak at λ_i begins to emerge, similarly to Fig. 2(a). A zoom around λ_0 (not shown) reveals that small satellite peaks at both sides of the large peak appear at ± 6.3 GHz, corresponding to the relaxation oscillation

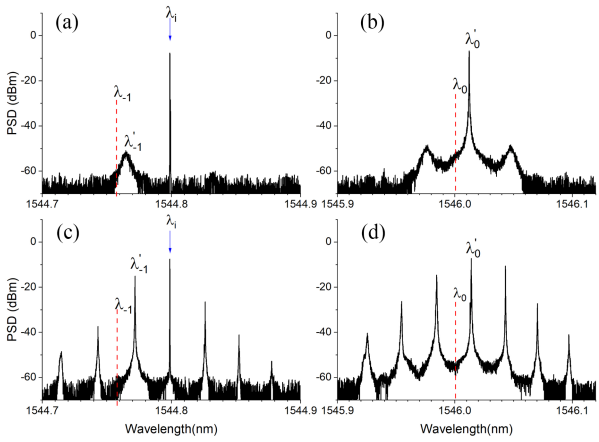

Fig. 6. Optical spectra at $\Delta\nu_{-1} = -5.2$ GHz for (a)–(b) $P_i = 84.9\ \mu$W, (c)–(d) $P_i = 134.6\ \mu$W. Parts (a)–(b) (c)–(d) correspond to zooms of Fig. 5(b) and (c).

frequency. Several peaks with wavelengths close to those of the $q = -2, -1, 0$, and 1 longitudinal modes are excited when P_i is increased to 84.9 μW, as illustrated in Fig. 5(b). Zooms of Fig. 5(b) around $q = -1$ and $q = 0$ modes are shown in Fig. 6(a) and (b), respectively. The wavelengths of the longitudinal modes of the solitary laser, λ_{-1} and λ_0 are also indicated with vertical dashed lines. The wavelength redshift due to OI is well illustrated in Fig. 6(a) and (b) since λ'_{-1} and λ'_0 are around 0.01 nm longer than λ_{-1} and λ_0, respectively. Fig. 6(b) shows that the satellite peaks no longer appear at ± 0.048 nm (± 6.3 GHz) distance from λ'_0 but at smaller distance ± 0.36 nm (± 4.5 GHz) that is precisely the wavelength difference shown in Fig. 6(a), $\lambda_i - \lambda'_{-1}$. Fig. 5(c) and its corresponding zooms in Fig. 6(c) and (d) show that multiple peaks appear in the spectrum close to the $q = -1$ and $q = 0$ modes when P_i increases. Consecutive peaks are separated by 3.4 GHz, both in Fig. 6(c) and (d). Fig. 6(c) shows that the wavelength resonance approaches λ_i because P_i has increased. This leads to the excitation of the $q = -1$ longitudinal mode at λ'_{-1} accompanied by the appearance of another five lines with a constant separation between them of 3.4 GHz. The spectrum around λ'_0 shown in Fig. 6(d) is similar to that shown in Fig. 6(c) also with a separation between consecutive peaks of 3.4 GHz. In this way the beating between the optical injection and the $q = -1$ mode causes a similar oscillation in the $q = 0$ mode.

Fig. 5(d) shows that increasing the value of P_i leads to a smaller separation (2.25 GHz) between λ_i and λ'_{-1} with the appearance of much more peaks around λ_i and with a more irregular structure that translates also to the spectrum around λ'_0. In Fig. 5(e) the above mentioned separation is just 1 GHz and the spectrum around both modes is irregular showing a broad pedestal. Increasing slightly P_i with respect to Fig. 5(e) leads to a sudden transition to the locked state as illustrated in Fig. 5(f).

Fig. 7 shows the optical spectra obtained for a positive frequency detuning with respect to the $q = -1$ longitudinal mode. These are obtained for $\lambda_i = 1544.71$ nm, for which $\Delta\nu_{-1} = 6.1$ GHz ($\Delta\lambda_{-1} = -0.048$ nm) and several values of P_i. When P_i is very small a weak peak at λ_i appears as shown in Fig. 7(a).

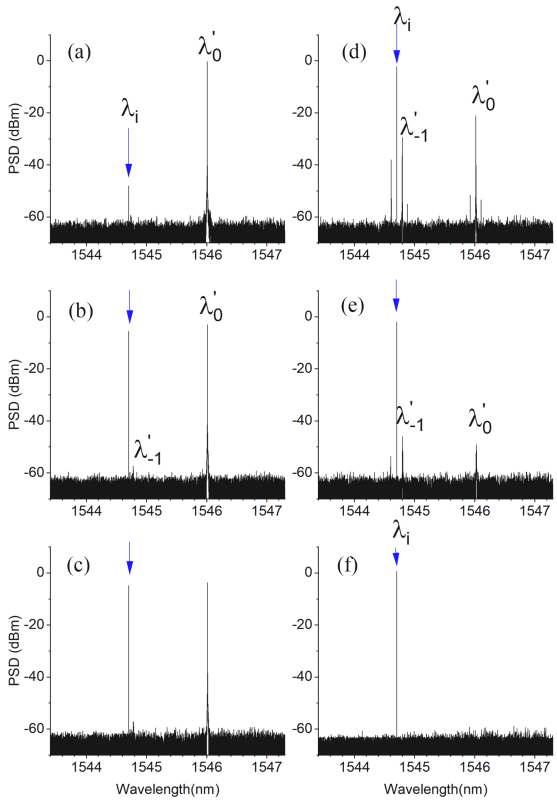

Fig. 7. Optical spectra at $\Delta\nu_{-1} = 6.1$ GHz for (a) $P_i = 7.3$ nW, (b) $P_i = 134.6\ \mu$W, (c) $P_i = 194.6\ \mu$W, (d) $P_i = 488.8\ \mu$W, (e) $P_i = 674.8\ \mu$W, and (f) $P_i = 8.2$ mW. The injection wavelength is indicated with an arrow.

As P_i increases that peak significantly increases and a tiny peak corresponding to λ'_{-1} begins to appear, as shown in Fig. 7(b) and (c). The wavelength of that peak increases with P_i as expected (1544.78 nm and 1544.785 nm in Fig. 7(b) and (c), respectively). The magnitude of the peak at λ'_{-1} is so small that is not able to induce any observable dynamics in the $q = 0$ mode. That dynamics is observed in Fig. 7(d), corresponding to a substantial increase of P_i. In this figure $\lambda'_{-1} = 1544.797$ nm for which $\Delta\nu'_{-1} = 11.6$ GHz. In this case the peak at λ'_{-1} and satellite peaks around λ_i, separated by 11.6 GHz, are excited. Periodic dynamics with 11.6 GHz repetition frequency are then observed in both longitudinal modes although the magnitude of the peak at λ'_0 has significantly decreased with respect to Fig. 7(c). Fig. 7(e) and (f) shows that increasing P_i leads to the disappearance of the emission of the $q = 0$ mode until complete locking is obtained.

V. Effect of the Optical Injection on the GS-OFC Generated in the DML

In this section we analyze the effect of the optical injection in OFCs generated by gain-switching our DML. We consider the strong injection conditions of Fig. 3 for which we have obtained a very wide locking range, more than 37 nm. Similar strong injection conditions (13.5 dBm power emitted by the tunable laser, like in our case) were considered for a gain-switched FP laser for which a quasi-continuous wavelength tunability of 31 nm was shown [40]. We apply a sinusoidal modulation

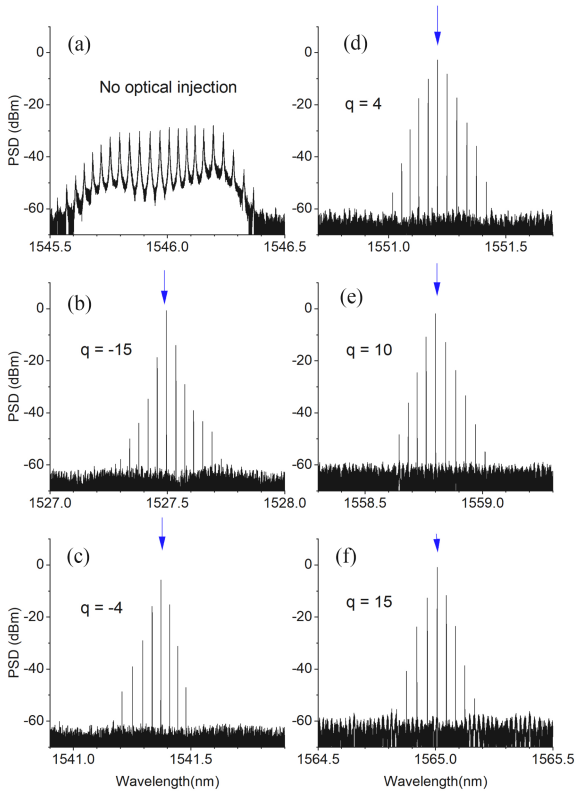

Fig. 8. Optical spectra of the DML when RF signal with $f_R = 5$ GHz and a modulation voltage of $V_{RF} = 1.5$ V is applied for (a) no optical injection, and with optical injection with $P_i = 8.2$ mW and (b) $\lambda_i = 1527.49$ nm ($\Delta\lambda_{-15} = -0.074$ nm), (c) $\lambda_i = 1541.37$ nm ($\Delta\lambda_{-4} = 0.329$ nm), (d) $\lambda_i = 1551.22$ nm ($\Delta\lambda_4 = 0.227$ nm), (e) $\lambda_i = 1558.8$ nm ($\Delta\lambda_{10} = 0.258$ nm), and (f) $\lambda_i = 1565$ nm ($\Delta\lambda_{15} = 0.111$ nm). The injection wavelength is indicated with an arrow.

current with a repetition frequency of $f_R = 5$ GHz, a modulation voltage, $V_{RF} = 1.1$ V, and $I_{bias} = 30$ mA. Fig. 8(a) shows the optical spectrum of the free-running GS-DML. This spectrum corresponds to an OFC in which the frequency separation between consecutive lines is 5 GHz. The laser is not completely switched-off between pulses in such a way that temporal coherence is preserved and an OFC is formed. A good-quality OFC is formed with a relatively small value of V_{RF} since we have chosen a small value of I_{bias} [39]. In the rest of spectra of Fig. 8 we show the results obtained when optical injection is applied under the same conditions considered in Fig. 3. We obtain locked OFCs for all the longitudinal modes for which we observed locking under CW-operation of the DML. In all the spectra the line with maximum strength appears at λ_i. Another indication of locking operation is the signal level between lines that is of the order of the noise floor of our spectrum analyzer. The carrier to noise ratios [39] of optical spectra in Fig. 8(b)–(f) are much larger than that of Fig. 8(a) indicating phase correlation of the emitted pulses, good pulse-to-pulse phase stability, and a significant reduction in the linewidth (the linewidth of our tunable laser, 75 kHz, is much smaller than the linewidth of the DML). Another characteristic of our locked OFCs is that the spectral width of the comb is smaller than that of the solitary laser. This has also been observed when injecting with high strength close to the $q = 0$ mode in a DML (see for instance Fig. 3 in [48]). Summarizing, our results show that injection locked gain-switched OFCs are obtained in DMLs with a quasi-continuous wavelength tunability of more than 37 nm [40].

VI. Discussion and Conclusions

Optical injection experiments in single-mode semiconductor lasers have been mainly focused on DFB devices in which the injected wavelength is close to that of the free-running longitudinal mode. Under these conditions the results are very similar to those obtained with DMLs. However we would expect very different results for both devices when considering OI far from the free-running mode due to the very different dependence of the photon lifetime on the wavelength. In DFB and DML devices the photon lifetime has a maximum close to the free-running longitudinal mode wavelength, $q = 0$, [9], [52]. However while the photon lifetime remains constant for modes with $q \neq 0$ in DMLs [9], there is a monotonous decrease of that value as $\mid q \mid$ increases in DFBs [52]. This is the reason why we would not expect to observe injection locking of longitudinal modes with $q \neq 0$ in DFBs. We also note that the photon lifetime is constant for all modes in Fabry-Perot lasers and therefore injection locking of longitudinal modes with large values of $\mid q \mid$ are observed [40] like in our case.

In our experiment the range of wavelengths in which injection locking has been observed is limited by the wavelength span of our optical spectrum analyzer. We would expect that this range is larger and would be limited by the width of the gain spectrum. In fact, very recently a 60 nm tunable slotted Fabry-Perot laser has been demonstrated [53].

To summarize, we have reported measurements of the effect of the optical injection on a single longitudinal mode DML when the injected wavelength is far from that of the solitary device. We have shown that injection locking of many longitudinal modes is obtained in a very wide wavelength range (larger than 37 nm), similarly to Fabry Perot lasers [40], and limited by our measurement equipment. We have found that the injection locking range is minimum when injecting around the free-running mode of the DML. We have presented the nonlinear dynamics of the DML when the injected wavelength is close to a longitudinal mode different from the free-running mode. We have shown that different dynamics simultaneously appear in several modes depending on the sign of the frequency detuning, a feature that cannot arise in the conventional injection of the central, free-running lasing mode. Finally, we have shown that wavelength tunable injection-locked optical frequency combs are obtained with a free spectral range of 5 GHz and quasi-continuous wavelength tunability larger than 37 nm.

Acknowledgment

The authors would like to thank Ignacio Esquivias for useful comments.

References

[1] L. F. De Chiaro, "Damage-induced spectral perturbations in multi-longitudinal-mode semiconductor lasers," *J. Lightw. Technol.*, vol. 8, no. 11, pp. 1659–1669, Nov. 1990.

[2] B. Corbett and D. McDonald, "Single longitudinal mode ridge waveguide 1.3 μm Fabry-Perot laser by modal perturbation," *Electron. Lett.*, vol. 31, no. 25, pp. 2181–2182, 1995.

[3] S. O'Brien and E. P. O'Reilly, "Theory of improved spectral purity in index patterned Fabry-Perot lasers," *Appl. Phys. Lett.*, vol. 86, no. 20, 2005, Art. no. 201101.

[4] B. Kelly et al., "Discrete mode laser diodes with very narrow linewidth emission," *Electron. Lett.*, vol. 43, no. 23, 2007, pp. 1282–1284.

[5] D. C. Byrne et al., "Discretely tunable semiconductor lasers suitable for photonic integration," *IEEE J. Sel. Topics Quantum Electron.*, vol. 15, no. 3, pp. 482–487, May/Jun. 2009.

[6] S. O'Brien et al., "Design, characterization, and applications of index-patterned Fabry–Pérot lasers," *IEEE J. Sel. Topics Quantum Electron.*, vol. 17, no. 6, pp. 1621–1631, Nov./Dec. 2011.

[7] V. Weldon, K. Boylan, B. Corbett, D. McDonald, and J. O'Gorman, "A novel single frequency stabilized Fabry–Perot laser diode at 1590 nm for gas sensing," *Spectrochimica Acta Part A: Mol. Biomol. Spectrosc.*, vol. 58, no. 11, pp. 2433–2438, 2002.

[8] K. Shi et al., "Fast switching slotted Fabry–Perot laser for phase modulated transmission systems," *J. Lightw. Technol.*, vol. 28, no. 23, pp. 3409–3416, Dec. 2010.

[9] N. D. Boohan, B. Corbett, and E. P. O'Reilly, "Robust single frequency index-patterned laser design using a Fourier design method," *Opt. Exp.*, vol. 31, no. 7, pp. 11536–11546, 2023.

[10] C. Guignard et al., "Low sensitivity to optical feedback and optical injection of discrete mode lasers," in *Proc. 19th Annu. Meeting IEEE Lasers Electro- Opt. Soc.*, 2006, pp. 663–664.

[11] Y. Tang et al., "Narrow-linewidth GAN-on-SI laser diode with slot gratings," *Nanomaterials*, vol. 11, no. 11, 2021, Art. no. 3092.

[12] T. Thiessen et al., "Back-side-on-BOX heterogeneously integrated III-V-on-silicon O-band distributed feedback lasers," *J. Lightw. Technol.*, vol. 38, no. 11, pp. 3000–3006, Jun. 2020.

[13] R. Lang, "Injection locking properties of a semiconductor laser," *IEEE J. Quantum Electron.*, vol. 18, no. 6, pp. 976–983, Jun. 1982.

[14] S. Wieczorek, B. Krauskopf, T. B. Simpson, and D. Lenstra, "The dynamical complexity of optically injected semiconductor lasers," *Phys. Rep.*, vol. 416, pp. 1–128, 2005.

[15] S.-C. Chan, "Analysis of an optically injected semiconductor laser for microwave generation," *IEEE J. Quantum Electron.*, vol. 46, no. 3, pp. 421–428, Mar. 2010.

[16] T. Fortier and E. Baumann, "20 years of developments in optical frequency comb technology and applications," *Commun. Phys.*, vol. 2, no. 1, pp. 1–16, 2019.

[17] M. Imran, P. M. Anandarajah, A. Kaszubowska-Anandarajah, N. Sambo, and L. Poti, "A survey of optical carrier generation techniques for terabit capacity elastic optical network," *IEEE Commun. Surveys Tuts.*, vol. 20, pp. 211–263, Firstquarter, 2018.

[18] J. Pfeifle et al., "Flexible terabit/s Nyquist-WDM super-channels using a gain-switched comb source," *Opt. Exp.*, vol. 23, pp. 724–738, 2015.

[19] C. Browning et al., "Gain-switched optical frequency combs for future mobile radio-over-fiber millimeter-wave systems," *J. Lightw. Technol.*, vol. 36, no. 19, pp. 4602–4610, 2018.

[20] P. Trocha et al., "Ultrafast optical ranging using microresonator soliton frequency combs," *Science*, vol. 359, no. 6378, pp. 887–891, 2018.

[21] G. B. Rieker et al., "Frequency-comb-based remote sensing of greenhouse gases over kilometer air paths," *Optica*, vol. 1, no. 5, pp. 290–298, 2014.

[22] P. Martin-Mateos, M. Ruiz-Llata, J. Posada-Roman, and P. Acedo, "Dual-comb architecture for fast spectroscopic measurements and spectral characterization," *IEEE Photon. Technol. Lett.*, vol. 27, no. 12, pp. 1309–1312, Jun. 2015.

[23] S. T. Cundiff and A. M. Weiner, "Optical arbitrary waveform generation," *Nature Photon.*, vol. 4, no. 11, 2010, Art. no. 760.

[24] V. Torres-Company and A. M. Weiner, "Optical frequency comb technology for ultra-broadband radio-frequency photonics," *Laser Photon. Rev.*, vol. 8, no. 3, pp. 368–393, 2014.

[25] J. Pfeifle et al., "Coherent terabit communications with microresonator Kerr frequency combs," *Nature Photon.*, vol. 8, no. 5, pp. 375–380, 2014.

[26] P.-T. Ho, L. Glasser, E. Ippen, and H. Haus, "Picosecond pulse generation with a CW GaAlAs laser diode," *Appl. Phys. Lett.*, vol. 33, no. 3, pp. 241–242, 1978.

[27] P. Anandarajah et al., "Generation of coherent multicarrier signals by gain switching of discrete mode lasers," *IEEE Photon. J.*, vol. 3, no. 1, pp. 112–122, Feb. 2011.

[28] P. M. Anandarajah et al., "Phase shift keyed systems based on a gain switched laser transmitter," *Opt. Exp.*, vol. 17, pp. 12668–12677, 2009.

[29] V. Vujicic, P. M. Anandarajah, R. Zhou, C. Browning, and L. P. Barry, "Performance investigation of IM/DD compatible SSB-OFDM systems based on optical multicarrier sources," *IEEE Photon. J.*, vol. 6, no. 5, Oct. 2014, Art. no. 7903110.

[30] P. M. Anandarajah, S. P. Ó. Dúill, R. Zhou, and L. P. Barry, "Enhanced optical comb generation by gain-switching a single-mode semiconductor laser close to its relaxation oscillation frequency," *IEEE J. Sel. Topics Quantum Electron.*, vol. 21, no. 6, pp. 592–600, Nov./Dec. 2015.

[31] S. P. O. Dúill, R. Zhou, P. M. Anandarajah, and L. P. Barry, "Analytical approach to assess the impact of pulse-to-pulse phase coherence of optical frequency combs," *IEEE J. Quantum Electron.*, vol. 51, no. 11, 2015, Art. no. 1200208.

[32] S. P. O. Dúill, P. M. Anandarajah, R. Zhou, and L. P. Barry, "Numerical investigation into the injection-locking phenomena of gain switched lasers for optical frequency comb generation," *Appl. Phys. Lett.*, vol. 106, no. 21, 2015, Art. no. 211105.

[33] A. R. Criado, C. de Dios, E. Prior, M. Ortsiefer, P. Meissner, and P. Acedo, "VCSEL-based optical frequency combs: Toward efficient single-device comb generation," *IEEE Photon. Technol. Lett.*, vol. 25, no. 20, pp. 1981–1984, Oct. 2013.

[34] E. Prior, C. De Dios, M. Ortsiefer, P. Meissner, and P. Acedo, "Understanding VCSEL-based gain switching optical frequency combs: Experimental study of polarization dynamics," *J. Lightw. Technol.*, vol. 33, no. 22, pp. 4572–4579, 2015.

[35] B. Jerez, P. Martin-Mateos, E. Prior, C. de Dios, and P. Acedo, "Dual optical frequency comb architecture with capabilities from visible to mid-infrared," *Opt. Exp.*, vol. 24, pp. 14986–14994, 2016.

[36] S. Chandran, S. Mahon, A. A. Ruth, J. Braddell, and M. D. Gutierrez, "Cavity-enhanced absorption detection of H_2S in the near-infrared using a gain-switched frequency comb laser," *Appl. Phys. B*, vol. 124, pp. 63–71, 2018.

[37] A. Rosado, A. Pérez-Serrano, J. M. G. Tijero, A. Valle, L. Pesquera, and I. Esquivias, "Experimental study of optical frequency comb generation in gain-switched semiconductor lasers," *Opt. Laser Technol.*, vol. 108, pp. 542–550, 2018.

[38] A. Rosado, A. Pérez-Serrano, J. M. G. Tijero, A. Valle, L. Pesquera, and I. Esquivias, "Enhanced optical frequency comb generation by pulsed gain-switching of optically injected semiconductor lasers," *Opt. Exp.*, vol. 27, pp. 9155–9163, 2019.

[39] A. Rosado, A. Pérez-Serrano, J. M. G. Tijero, A. Valle, L. Pesquera, and I. Esquivias, "Numerical and experimental analysis of optical frequency comb generation in gain-switched semiconductor lasers," *IEEE J. Quantum Electron.*, vol. 55, no. 6, Dec. 2019, Art. no. 2001012.

[40] G. Jain, D. Gutierrez-Pascual, M. J. Wallace, J. F. Donegan, and P. M. Anandarajah, "Experimental investigation of external optical injection and its application in gain-switched wavelength tunable optical frequency comb generation," *J. Lightw. Technol.*, vol. 39, no. 18, pp. 5884–5895, 2021.

[41] F. A. Gutiérrez, E. P. Martin, P. Perry, A. D. Ellis, P. M. Anandarajah, and L. P. Barry, "WDM orthogonal subcarrier multiplexing," *J. Lightw. Technol.*, vol. 34, no. 8, pp. 1815–1823, 2015.

[42] L. N. Venkatasubramani et al., "CCO-OFDM for bandwidth-reconfigurable optical interconnects using gain-switched comb," *OSA Continuum*, vol. 3, no. 10, pp. 2925–2934, 2020.

[43] R. Karembera and T. Gibbon, "Effects of optical local oscillator power on the network bit error rate in optical heterodyning of comb lines from a gain-switched VCSEL comb," *Opt. Laser Technol.*, vol. 139, 2021, Art. no. 106955.

[44] A. R. Criado et al., "Continuous-wave sub-THz photonic generation with ultra-narrow linewidth, ultra-high resolution, full frequency range coverage and high long-term frequency stability," *IEEE Trans. Terahertz Sci. Technol.*, vol. 3, no. 4, pp. 461–471, Jul. 2013.

[45] W. Weng, A. Kaszubowska-Anandarajah, J. Liu, P. M. Anandarajah, and T. J. Kippenberg, "Frequency division using a soliton-injected semiconductor gain-switched frequency comb," *Sci. Adv.*, vol. 6, no. 39, 2020, Art. no. eaba2807.

[46] A. Rosado, M. R. Fernández-Ruiz, P. Corredera, J. M. G. Tijero, and I. Esquivías, "High-density and broad band optical frequency combs generated by pseudo-random phase modulation of optically injected gain-switched semiconductor lasers," *Opt. Laser Technol.*, vol. 163, 2023, Art. no. 109312.

[47] R. Zhou, T. N. Huynh, V. Vujicic, P. M. Anandarajah, and L. P. Barry, "Phase noise analysis of injected gain switched comb source for coherent communications," *Opt. Exp.*, vol. 22, no. 7, pp. 8120–8125, 2014.

[48] A. Quirce et al., "Nonlinear dynamics induced by optical injection in optical frequency combs generated by gain-switching of laser diodes," *IEEE Photon. J.*, vol. 12, no. 4, Aug. 2020, Art. no. 1503314.
[49] H. Zhu, R. Wang, T. Pu, P. Xiang, J. Zheng, and T. Fang, "A novel approach for generating flat optical frequency comb based on externally injected gain-switching distributed feedback semiconductor laser," *Laser Phys. Lett.*, vol. 14, no. 2, 2016, Art. no. 026201.
[50] L. Fan et al., "Tunable ultra-broadband microwave frequency combs generation based on a current modulated semiconductor laser under optical injection," *IEEE Access*, vol. 5, pp. 17764–17771, 2017.
[51] P. Anandarajah et al., "Discrete mode lasers for communication applications," *IET Optoelectron.*, vol. 3, pp. 1–17, 2009.
[52] L. A. Coldren, S. W. Corzine, and M. L. Mashanovitch, *Diode Lasers and Photonic Integrated Circuits*, vol. 218. Hoboken, NJ, USA: Wiley, 2012.
[53] J. Mulcahy, J. McCarthy, F. H. Peters, and X. Dai, "60 nm widely tunable three section slot laser," *IEEE J. Quantum Electron.*, vol. 59, no. 6, Dec. 2023, Art. no. 2000706.

Ana Quirce received the Licenciada en Física (M.Sc.) and Ph.D. degrees in sciences, technologies, and computing in 2008 and 2012, respectively, from the University of Cantabria, Santander, Spain, where she was studying the dynamics of the polarization and transverse modes of vertical cavity surface-emitting lasers (VCSELs) subject to optical injection. She is currently a Beatriz-Galindo Reasercher with the Instituto de Fésica de Cantabria, Santander, Spain. Her research interests include the areas of dynamics of VCSELs, optical injection effects in semiconductor lasers, optical feedback, optical frequency combs, and photonic integrated circuits.

Bryan Kelleher received the Ph.D. degree from University College Cork, Cork, Ireland, in 2003. He is currently a Senior Lecturer with the School of Physics, University College Cork, and an Academic Member of Tyndall National Institute. His research interests include the dynamics of optically coupled lasers, quantum dot lasers, optical frequency combs, and photonic integrated circuits.

Angel Valle received the M.Sc. and Ph.D. degrees in physics from the Universidad de Cantabria, Santander, Spain, in 1988 and 1993, respectively. During 1994 and 1995, he was a Postdoctoral Fellow with the School of Electronic and Electrical Engineering, University of Bath, Bath, U.K. In 1996, he joined the Instituto de Física de Cantabria (CSIC-UC), Santander, Spain. Since 1998, he has been a Lecturer with the Departamento de Física Moderna, University of Cantabria, Spain. His research interests include the areas of vertical-cavity surface-emitting lasers, noise, and nonlinear dynamics of semiconductor lasers.